Sonication-Assisted Synthesis of CdS Quantum-Dot-Sensitized TiO2 Nanotube Arrays with Enhanced Photoelectrochemical and Photocatalytic Activity

ARTICLE *in* ACS APPLIED MATERIALS & INTERFACES · OCTOBER 2010

Impact Factor: 6.72 · DOI: 10.1021/am100605a · Source: PubMed

4 AUTHORS:

Yi Xie
Istituto Italiano di Tecnologia
23 PUBLICATIONS **726** CITATIONS
SEE PROFILE

Ghafar Ali
Korea Advanced Institute of Science and T…
49 PUBLICATIONS **591** CITATIONS
SEE PROFILE

Seung Hwa Yoo
Korea Advanced Institute of Science and T…
17 PUBLICATIONS **465** CITATIONS
SEE PROFILE

Sung Oh Cho
Korea Advanced Institute of Science and T…
114 PUBLICATIONS **2,101** CITATIONS
SEE PROFILE

ARTICLE

Sonication-Assisted Synthesis of CdS Quantum-Dot-Sensitized TiO_2 Nanotube Arrays with Enhanced Photoelectrochemical and Photocatalytic Activity

Yi Xie, Ghafar Ali, Seung Hwa Yoo, and Sung Oh Cho*

Department of Nuclear and Quantum Engineering, Korea Advanced Institute of Science and Technology (KAIST), 373-1 Guseong, Yuseong, Daejeon 305-701, Republic of Korea

ABSTRACT A sonication-assisted sequential chemical bath deposition (S-CBD) approach is presented to uniformly decorate CdS quantum dots (QDs) on self-organized TiO_2 nanotube arrays (TNTAs). This approach avoids the clogging of CdS QDs at the TiO_2 nanotube mouth and promotes the deposition of CdS QDs into the nanotubes as well as on the tube walls. The photoelectrochemical and photocatalytic properties of the resulting CdS-decorated TNTAs were explored in detail. In comparison with a classical S-CBD approach, the sonication-assisted technique showed much enhancement in the photoelectrochemical and photocatalytic activities of the CdS QDs-sensitized TNTAs.

KEYWORDS: TiO_2 nanotube arrays • CdS • chemical bath deposition • photoelectrochemistry • photocatalyst • visible light

1. INTRODUCTION

One-dimensional TiO_2 nanostructures, particularly TiO_2 nanotube arrays (TNTAs), have received great attention because of their superior photocatalytic and photoelectronic performance over TiO_2 nanopaticles (NPs) (1, 2). Since Zwilling et al. reported the growth of TiO_2 nanotubes (NTs) through the electrochemical anodization of Ti foil (3), many results on TNTAs have been reported to control the length, morphology, orientation, and pore size of the TNTAs by tailoring the electrochemical conditions during Ti anodization (4, 5). TNTAs have good photon-induced properties and facilitate the separation of the photoexcited charges and thus they are widely used as photocatalysts (1, 6) and photoanodes (7) to effectively harvest sunlight.

However, one of the critical drawbacks of TiO_2 is its wide band gap of 3.2 eV. That is, only ultraviolet (UV) region with the wavelength below ~390 nm of the solar spectrum can be utilized by pure TiO_2. To improve the photocatalytic efficiency, many efforts including dye sensitization (8), doping by nonmetals (9, 10), coupling with low band gap semiconductors such as PbS (11), CdTe (12), CdSe (13), and CdS (14−20) have been taken to extend the optical absorption into visible-light region. Among them, decoration of TNTAs with CdS has been considered to be an important technique because CdS has a narrow band gap and its conduction band level is higher than that of TiO_2.

To date, various approaches have been reported to decorate TNTAs with CdS, such as sequential chemical bath deposition (S-CBD) or successive ionic layer adsorption and reaction (SILAR) (16), electrochemical deposition (18), or using a bifunctional organic linker (19). Among them, S-CBD technique is the most straightforward, and CdS-TNTAs fabricated by this technique exhibited greatly enhanced photoactivities under visible irradiation (20). However, when an aqueous solution of the CdS precursors is used for sensitizing TNTAs, the precipitation reaction is so sudden that large agglomerates of CdS nanoparticles (NPs) are formed on the top surface of TNTAs, which block the tube mouths. In addition, the precursor solution tends not to penetrate fully the inner side of TiO_2 NTs because of a surface tension of the solution. As a result, both the inside surface and the bottom surface of the tubes are not fully decorated with CdS NPs, which thereby weakens the harvest of light for photocatalysis or solar cells.

Here, we present a novel sonication-assisted S-CBD technique to prepare CdS quantum dots (QDs) sensitized TNTAs. Compared to a typical S-CBD technique, the sonication-assisted S-CBD approach facilitates the deposition of CdS QDs inside the TiO_2 NTs and on the tube walls. The CdS QDs-sensitized TNTAs prepared by the sonication-assisted S-CBD technique exhibit much better photoelectrochemical and photocatalytic activities than those fabricated by a conventional S-CBD technique.

2. MATERIALS AND METHODS

2.1. Chemicals. Titanium foil (99.6% purity, 0.1 mm thick) was purchased from Goodfellow (England). Cadmium chloride 2.5-hydrate was obtained from Kanto Chemical Co. (Japan). Ammonium fluoride (NH_4F) and sodium sulfide nonahydrate

* Corresponding author. Tel: +82-42-350-3823. Fax: +82-42-350-3810. E-mail: socho@kaist.ac.kr.
Received for review July 11, 2010 and accepted September 3, 2010
DOI: 10.1021/am100605a

Published on Web 09/17/2010

were available from Sigma-Aldrich (USA) and ethylene glycol was purchased from Junsei Chemical Co. (Japan).

2.2. Synthesis of TNTAs. Self-organized TNTAs were fabricated by anodization of Ti foils in ethylene glycol (94.5 wt %) solution with additions of 0.5 wt % of NH_4F and 5.0 wt % of deionized (DI) water. Prior to the anodization, Ti foils were sonicated successively in acetone, isopropanol, and ethanol. The foils were subsequently rinsed with DI water and then dried in a N_2 stream. To obtain TNTAs, we immersed the degreased Ti foil ($2.5 \times 3.2 \times 0.01$ cm^3 in size) with a working area of 2.0×3.2 cm^2 in the as-prepared electrolyte. Anodization was carried out in a two electrodes cell containing a cathode of platinum (Pt) foil at 40 V under ambient temperature (18−20 °C). After 24 h of anodization, the sample removed from the electrode cell was washed with DI water and sonicated for 50−60 min to remove the surface debris. A subsequent heating at 400 °C for 3 h with a temperature ramp rate of 1 °C min^{-1} in air was applied to achieve the crystallization of TNTAs before the CdS deposition.

2.3. Synthesis of CdS-Sensitized TNTAs. CdS QDs were fabricated on the TNTAs by a sonication-assisted S-CBD approach. TNTAs were sequentially dipped in four different beakers for 2 min in each beaker during sonication. The first beaker contained 0.025 M cadmium chloride ($CdCl_2$), the next contained 0.025 M sodium sulfide (Na_2S) solution, and the other two contained DI water. The excess reagent was removed by washing with DI water. Such an immersion procedure was repeated for 15 cycles, producing yellow samples. The as-prepared yellow samples were dried in a N_2 stream and these samples will be designated as sonication-CdS/TNTAs. As a reference material for the comparison of the photoelectrochemical and photocatalytic activities, CdS-sensitized TNTAs were also fabricated using the same process without sonication; and the material was designated as CdS/TNTAs.

2.4. Materials Characterization. X-ray diffraction (XRD) measurements were obtained on a D/MAX-2500 diffractometer (Rigaku, Japan). The surface morphology and direct cross-section thickness measurements were carried out using a S-4800 field emission scanning electron microscopy (FESEM, Hitachi, Japan). The TNTAs coupled with CdS QDs were also characterized using a field emission transmission electron microscope (FETEM, Tecnai G2 F30, Netherland). Quantitative analysis was carried out with energy-dispersive X-ray spectroscopy (EDS) attached with the FETEM. UV−vis diffuse reflectance (DR) spectroscopy was recorded using a spectrometer UV−vis spectrometer equipped with a SA-13.1 diffuse reflector (Scinco S-4100, Korea).

2.5. Photoelectrochemical Measurements. Photoelectrochemical measurements were performed in a 300 mL rectangular quartz cell using a three electrode configuration, which were composed of the as-prepared sample as a working electrode, a Pt foil as a counter electrode, a saturated Ag/AgCl as a reference electrode, and 0.5 M Na_2S as an electrolyte. The working electrode was illuminated with a solar simulator equipped with a 200 W Xe lamp. An ultraviolet cutoff filter was inserted between the light source and the quartz cell to exclude UV light with the wavelength below 420 nm. The photocurrent dynamics of the working electrode were recorded according to the responses to sudden switching on and off at 0 V bias.

2.6. Photocatalytic Degradation of Methyl Orange. Methyl orange (MO) was considered as a model contaminant in the purification of dye wastewater. The fabricated TNTAs, CdS/TNTAs, and sonication-CdS/TNTAs were cut into the same size of 2.0 cm × 0.8 cm^2, and were vertically placed in the center of a rectangular quartz cell for photocatalytic degradation experiments. The quartz cell contained 2 mL of MO (9 mg/L) in a 0.2 M Na_2S solution. The visible light passing through the UV filter and the quartz window irradiated the front-side of the photocatalyst. The photocatalyst was 0.2 cm away from the quartz window. Before irradiation, the photocatalyst was immersed into a MO solution in a dark room for 30 min. The relative concentration of MO in the solution was determined by comparing its UV−vis absorption intensity with that of the initial MO solution at 464 nm.

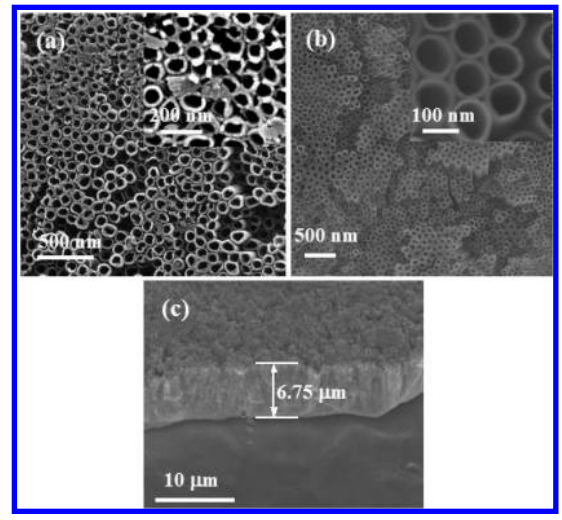

FIGURE 1. FESEM of TNTAs anodized at 40 V for 24 h: (a) as-anodized TNTAs, (b) TNTAs after remove the surface debris, and (c) cross-sectional image of TNTAs.

3. RESULTS AND DISCUSSION

3.1. Sample Characterization. Figure 1 shows the FESEM images of the TNTAs fabricated by anodization of Ti foils. The TNTAs were covered with a large amount of debris (Figure 1a), which could be removed by sonication cleaning in DI water (Figure 1b). TNTAs with an outer average diameter of 100 nm and inner average diameter of 80 nm were uniformly grown on Ti substrate. The average length of the NTs was about 6.75 μm (Figure 1c).

Figure S1 in the Supporting Information demonstrates the schematic representation of fabrication process of CdS QDs on TNTAs. The TNTAs were sequentially exposed to Cd^{2+} and S^{2-} ions by consecutive immersing of the TNTAs into the solutions of $CdCl_2$, water, Na_2S, and water while the solutions are sonicated. Because of the sonication, the Cd^{2+} and S^{2-} ions could diffuse and penetrate fully inner surface of the TiO_2 NTs (see Figure S1b in the Supporting Information). Consequently, a layer of CdS QDs could be formed on the inside NT's wall after several immersion cycles (see Figure S1c in the Supporting Information).

Images a and b in Figure 2 show the FESEM images of the CdS QDs-sensitized TNTAs prepared by the sonication-assisted S-BCD approach and the conventional S-BCD approach without sonication, respectively. The effectiveness of the sonication-assisted approach for depositing CdS QDs in the TiO_2 NTs is clearly seen from Figure 2. No obvious aggregates of CdS are observed at the entrances of TiO_2 NTs prepared via the sonication-assisted S-BCD approach (Figure 2a). However, CdS aggregates are clearly observed on the entrances of TiO_2 NTs fabricated without sonication assistance (Figure 2b). In the latter case, the CdS precursor solutions could not penetrate deeply into the TiO_2 NTs

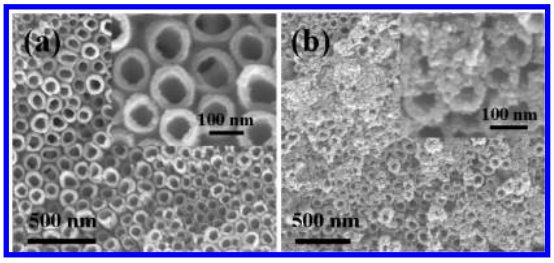

FIGURE 2. FESEM images of (a) CdS/TNTAs an (b)d sonication-CdS/TNTAs.

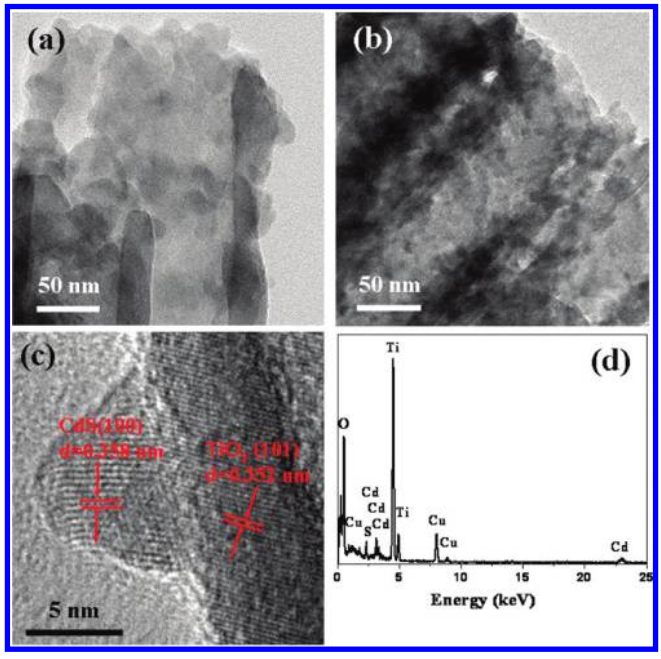

FIGURE 3. TEM images of (a) the CdS/TNTAs and (b) the sonication-CdS/TNTAs. (c) High-resolution TEM image and (d) EDS spectrum of the sonication-CdS/TNTAs.

because of surface tension of the solutions (see Figure S1d in the Supporting Information), resulting in the aggregates at the entrances of the NTs (see Figure S1e in the Supporting Information). In addition, sonication-CdS/TNTAs had a little larger wall thickness than that of bare TNTAs, because of the deposition of CdS on the tube walls. These results revealed that the sonication-assisted deposition approach is very effective for the decoration of TNTAs with CdS QDs.

The microscopic structure of the CdS QDs-sensitized TNTAs was further investigated by a FETEM. The TEM image of the CdS/TNTAs shows that large aggregates of CdS cover the entrance of the TNTAs (Figure 3a). However, The TEM image of the sonication-CdS/TNTAs clearly displays that CdS QDs were abundantly deposited inside the TNTAs (Figure 3b). Figure 3c provides a high-resolution TEM image of the sonication-CdS/TNTAs, which shows that a crystalline CdS quantum dot with the size of ~5 nm was grown on an anatase TiO_2 NT. The lattice distances shown in Figure 3c corresponds well with (101) plane of anatase TiO_2 and (100) plane of CdS, respectively. EDS spectrum of the sonication-CdS/TNTAs also demonstrates the presence of Ti, O, Cd, and S (Figure 3d). Moreover, quantitative analysis of the EDS

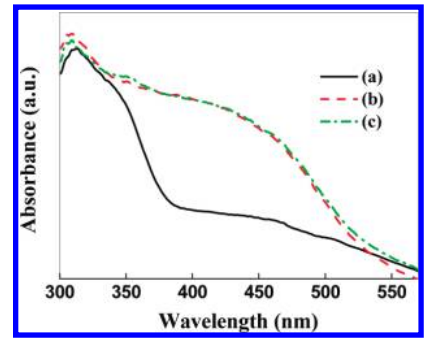

FIGURE 4. UV−vis diffuse reflectance absorption spectra of the (a) plain TNTAs, (b) CdS/TNTAs, and (c) sonication-CdS/TNTAs.

spectrum reveals that the molar ratio of Cd to S is close to 1:1, confirming the stoichiometric formation of CdS.

XRD patterns of the plain TNTAs and CdS-decorated TNTAs are shown in Figure S2. The XRD peaks of as-prepared TNTAs correspond to anatase TiO_2 (JCPDS card No. 21−1272) and titanium (JCPDS card No. 44−1294) (Figure S2a). In addition to these peaks, XRD peaks originating from hexagonal CdS (JCPDS card no. 41−1049) are also observed for CdS/TNTAs and sonication-CdS/TNTAs (see Figure S2b,c in the Supporting Information). These results further indicate that the TNTAs prepared by the sonication-assisted S-BCD approach are composed of CdS and TiO_2 crystalline structures.

UV−vis DR spectra of the plain TNTAs and CdS QDs-sensitized TNTAs reveal that pure TNTAs absorb mainly UV light with a wavelength below 400 nm (Figure 4a), whereas the absorption spectra of the CdS-sensitized TNTAs extend into the visible region (Figure 4b, c). The absorption edge of the CdS-sensitized TNTAs is ~530 nm, indicating that deposition of CdS QDs significantly improved the visible light absorption property of the TNTAs. Furthermore, the absorbance in the visible region of sonication-CdS/TNTAs is a little stronger than that of CdS/TNTAs. The band gap energies of the TNTAs can be obtained using the graphs of transformed Kubelka−Munk function (21), which are shown in the inset of Figure S3 in the Supporting Information. The band gap of the plain TNTAs is estimated to be 3.03 eV, which is a little lower than that of bulk anatase TiO_2. The band gaps of both the CdS/TNTAs and the sonication-CdS/TNTAs are calculated to be ~2.20 eV. In addition, the absorption peaks of the CdS-sensitized TNTAs are blue-shifted compared to those of CdS NPs prepared under the same conditions (not shown here), suggesting the effective electronic interaction between TNTAs and CdS QDs.

3.2. Photoelectrochemical Behaviors. A comparison between the photoelectrochemical behavior of as-synthesized TNTAs and CdS QDs-sensitized TNTAs was made using a three-electrode photoelectrochemical cell. Figure 5 provides the photocurrent responses of the TNTAs under a 0 V bias vs Ag/AgCl reference electrode. The plain TNTAs show very low photocurrent density under visible irradiation, and sonication-CdS/TNTAs exhibits much higher photocurrent density than that of CdS/TNTAs. The average photocurrent densities are 0.024, 1.43, and 2.06 mA/cm^2 for plain TNTAs, CdS/TNTAs, and sonication-CdS/TNTAs,

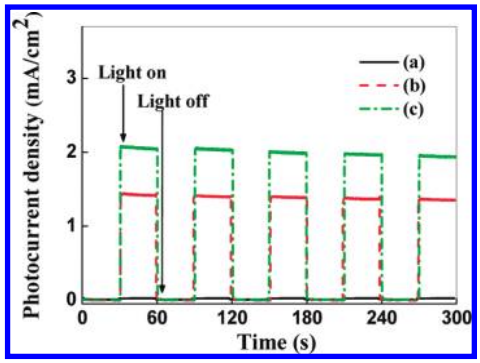

FIGURE 5. Photocurrent response of (a) plain TNTAs, (b) CdS/TNTAs, (c) sonication-CdS/TNTAs under visible illumination at the bias voltage of 0 V.

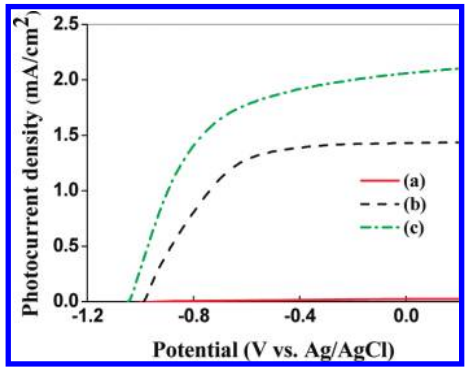

FIGURE 6. Current−voltage curves of (a) plain TNTAs, (b) CdS/TNTAs, and (c) sonication-CdS/TNTAs under visible illumination.

respectively. These results demonstrate that the CdS-sensitized TNTAs fabricated by sonication-assisted S-CBD technique harvest visible light more efficiently than those prepared by classical S-CBD approach.

Meanwhile, current−voltage ($I-V$) curves of the samples are further measured under visible light irradiation (Figure 6), which further confirms the photocurrent density of the sonication-CdS/TNTAs is much higher than those of CdS/TNTAs and plain TNTAs. The photocurrent onset occurred at −0.93 V for the as-synthesized TNTAs. However, the photocurrent onsets shift to −0.98 and −1.05 V for the CdS/TNTAs and the sonication-CdS/TNTAs, respectively. These results indicate that better charge separation and electron accumulation occur in the sonication-CdS/TNTAs than in CdS/TNTAs (22, 23), which is attributed to the fact that more dense CdS QDs were formed on the TiO_2 NTs by the assistance of sonication.

3.3. Photocatalytic Degradation of MO. Figure 7 shows the photodecomposition behavior of MO dye by plain TNTAs and CdS-sensitized TNTAs under visible irradiation ($\lambda \geq 420$ nm). The concentration of MO decreases with irradiation time because of the photodegradation. The ratio of MO concentration C/C_0 could be calculated as follows

$$C/C_0 = A/A_0 \quad (1)$$

where C_0 and C are the concentration of MO at irradiation time 0 and t, and A_0 and A are the absorbance values at the

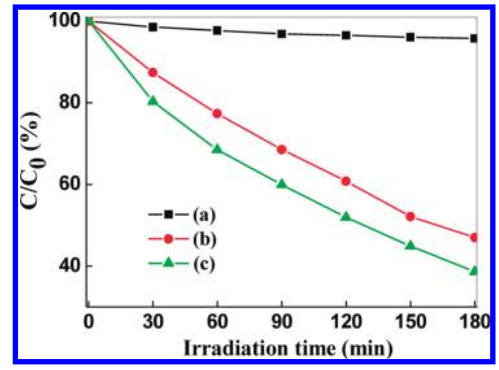

FIGURE 7. Visible-light-induced ($\lambda \geq 420$ nm) degradation behavior of MO over (a) plain TNTAs, (b) CdS/TNTAs, (c) sonication-CdS/TNTAs.

wavelength of 464 nm at time of 0 and t, respectively. After 180 min of visible irradiation, 61.4% of MO was decomposed by sonication-CdS/TNTAs, whereas 53.0 and 4.2% of MO was decomposed by CdS/TNTAs and plain TNTAs, respectively. This result shows that visible-light-induced catalytic efficiency of the CdS-sensitized TNTAs was improved by the sonication-assisted S-CBD technique.

3.4. Mechanism Discussion. The mechanism of the enhanced photocatalytic and photoelectrochemical properties of TiO_2 nanostructures decorated with low band gap semiconductors has been investigated in literatures (12, 18, 24, 25). When illuminated by visible light, CdS effectively excite electrons and holes (eq 2). The conduction band of TiO_2 NTs is more positive than that of CdS QDs, resulting in a local electric field. As a result, the excited electrons can quickly transfer from CdS QDs to TiO_2 conduction band (eq 3), whereas the generated holes accumulate in the valence band of CdS to form hole center. Consequently, the excited electron/hole pairs could be separated effectively, which contributed to the improvement of photoelectrochemical properties of CdS QDs-sensitized TNTAs.

However, the mechanism of enhanced photocatalysis is somewhat different with that of enhanced photocurrent. The tubular and crystal structure of TiO_2 is useful for separating and transferring generated electrons to the collector electrode (Ti substrate foil), which contributed to the increasing photocurrent density. However, in the case of photocatalysis, the accumulated electrons in the conduction band of TiO_2 can be transferred to oxygen to form H_2O_2 (eqs 4 and 5), which could be further reduced to hydroxyl radicals (eq 6). The formed hydroxyl radicals could further degrade or mineralize organic dye MO to end products (H_2O and CO_2) (eq 7). Furthermore, the holes accumulated in the valence band of CdS could be consumed by participating in reaction with MO molecules directly to form intermediates or mineralized products (eq 8).

$$CdS + h\nu \rightarrow CdS(e + h) \quad (2)$$

$$CdS(e) + TiO_2 \rightarrow CdS + TiO_2(e) \quad (3)$$

$$TiO_2(e) + O_2 \rightarrow TiO_2 + O_2^{\bullet -} \quad (4)$$

$$O^{\bullet -} + TiO_2(e) + H^+ \rightarrow H_2O_2 \quad (5)$$

$$H_2O_2 + O_2^{\bullet -} \rightarrow OH^{\bullet} + OH^- + O_2 \quad (6)$$

$$OH^{\bullet} + MO \rightarrow \text{degraded or mineralized products} \quad (7)$$

$$CdS(h) + MO \rightarrow \text{degraded or mineralized products} \quad (8)$$

As can be seen from Figures 5−7, the sonication-CdS/TNTAs exhibit much higher photocurrent density (Figure 5) and photocatalytic efficiency than CdS/TNTAs under visible illumination. As analyzed from SEM and TEM (Figures 2 and 3), CdS QDs-sensitized TNTAs prepared through sonication-assisted S-CBD approach led to a uniform and intimate coating of CdS QDs inside TNTAs. These uniform and intimate structures can not only efficiently increase the path length of light in the CdS layer but also facilitate charge separation. Furthermore, XRD results show that sonication assistance resulted in hexagonal peaks with a little higher intensity (see Figure S2 in the Supporting Information), indicating a higher degree of crystallinity. These factors contribute to the enhancement of photocatalytic activity of sonication-CdS/TNTAs.

4. CONCLUSIONS

CdS QDs-sensitized TNTAs were prepared by a sonication-assisted S-CBD approach. The incorporation of CdS QDs with TiO_2 NTs extends the absorption spectrum of the TiO_2 NTs significantly into visible region up to 550 nm. The sonication-assisted S-CBD technique effectively prevents clogging of CdS at the TiO_2 nanotube mouth, and consequently creates more uniform and intimate QDs-NTs structure compared to a conventional S-CBD approach. The CdS QDs-sensitized TiO_2 TNTAs prepared through the sonication-assisted S-CBD technique lead to more efficient separation of photogenerated electrons from CdS to TiO_2 NTs, and exhibit much enhanced photocurrent generation and photocatalytic efficiency. The sonication-assisted S-CBD technique described here might be used as a general approach to improve the photoelectrochemical and photocatalytic properties of wide band gap semiconductors coupled with narrow band gap semiconductors.

Acknowledgment. This work was supported by the Science and Technology (MEST)/Korea Science and Engineering Foundation (KOSEF) grant (Nuclear R&D Program, 2010-0026150).

Supporting Information Available: Schematic representation of fabrication process of CdS QDs on TNTAs; XRD patterns of various TNTAs; plot of Kubelka−Munk function to characterize the band gap energies of TNTAs (PDF). This material is available free of charge via the Internet at http://pubs.acs.org.

REFERENCES AND NOTES

(1) Zheng, Q.; Zhou, B. X.; Bai, J.; Li, L. H.; Jin, Z. J.; Zhang, J. L.; Li, J. H.; Liu, Y. B.; Cai, W. M.; Zhu, X. Y. *Adv. Mater.* **2008**, *20*, 1044–1049.
(2) Shankar, K.; Basham, J. I.; Allam, N. K.; Varghese, O. K.; Mor, G. K.; Feng, X. J.; Paulose, M.; Seabold, J. A.; Choi, K. S.; Grimes, C. A. *J. Phys. Chem. C* **2009**, *113*, 6327–6359.
(3) Zwilling, V.; Darque-Ceretti, E.; Boutry-Forveille, A.; David, D.; Perrin, M. Y.; Aucouturier, M. *Surf. Interface Anal.* **1999**, *27*, 629–637.
(4) Macák, J. M.; Tsuchiya, H.; Schmuki, P. *Angew. Chem., Int. Ed.* **2005**, *44*, 2100–2102.
(5) Chanmanee, W.; Watcharenwong, A.; Chenthamarakshan, C. R.; Kajitvichyanukul, P.; Tacconi, N. R.; Rajeshwar, K. *J. Am. Chem. Soc.* **2008**, *130*, 965–974.
(6) Tan, L. K.; Kumar, M. K.; An, W. W.; Gao, H. *ACS Appl. Mater. Interfaces* **2010**, *2*, 498–503.
(7) Mor, G. K.; Shankar, K.; Paulose, M.; Varghese, O. K.; Grimes, C. A. *Nano Lett.* **2005**, *5*, 191–195.
(8) Zhao, W.; Sun, Y.; Castellano, F. N. *J. Am. Chem. Soc.* **2008**, *130*, 12566–12567.
(9) Asahi, R.; Morikawa, T.; Ohwaki, T.; Aoki, K.; Taga, Y. *Science* **2001**, *293*, 269–271.
(10) Khan, S. U. M.; Al-Shahry, M.; Ingler, W. B. *Science* **2002**, *297*, 2243–2245.
(11) Hoyer, P.; Könenkamp, R. *Appl. Phys. Lett.* **1995**, *66*, 349–351.
(12) Gao, X. F.; Li, H. B.; Sun, W. T.; Chen, Q.; Tang, F. Q.; Peng, L. M. *J. Phys. Chem. C* **2009**, *113*, 7531–7535.
(13) Lee, H. J.; Wang, M. K.; Chen, P.; Gamelin, D. P.; Zakeeruddin, S. M.; Grätzel, M.; Nazeeruddin, M. K. *Nano Lett.* **2009**, *9*, 4221–4227.
(14) Okur, H. I.; Türker, Y.; Dag, O. *Langmuir* **2010**, *26*, 538–544.
(15) Lin, C. J.; Yu, Y. H.; Liou, Y. H. *Appl. Catal., B* **2009**, *93*, 119–125.
(16) Larramona, G.; Chone, C.; Jacob, A.; Sakakura, D.; Delatouche, B.; Pere, D.; Cieren, X.; Nagino, M.; Bayon, R. *Chem. Mater.* **2006**, *18*, 1688–1696.
(17) Hwang, J. Y.; Lee, S. A.; Lee, Y. H.; Seok, S. I. *ACS Appl. Mater. Interfaces* **2010**, *2*, 1343–1348.
(18) Wang, C. L.; Sun, L.; Yun, H.; Li, J.; Lai, Y. K.; Lin, C. J. *Nanotechnology* **2009**, *20*, 295601. (6pp).
(19) Kim, J. C.; Choi, J.; Lee, Y. B.; Hong, J. H.; Lee, J. I.; Yang, J. W.; Lee, W. I.; Hur, N. H. *Chem. Commun.* **2006**, *48*, 5024–5026.
(20) Chi, C. F.; Lee, Y. L.; Weng, H. S. *Nanotechnology* **2008**, *19*, 125704. (5pp).
(21) Orel, Z. C.; Gunde, M. K.; Orel, B. *Prog. Org. Coat.* **2006**, *30*, 59–66.
(22) Spanhel, L.; Weller, H.; Henglein, A. *J. Am. Chem. Soc.* **1987**, *109*, 6632–6635.
(23) Wood, A.; Giersig, M.; Mulvaney, P. *J. Phys. Chem. B* **2001**, *105*, 8810–8815.
(24) Baker, D. R.; Kamat, P. V. *Adv. Funct. Mater.* **2009**, *19*, 805–811.
(25) Hou, Y.; Li, X. Y.; Zou, X. J.; Quan, X.; Chen, G. H. *Environ. Sci. Technol.* **2009**, *43*, 858–863.

AM100605A